

Turbulent Jet: A DNS Study

Sachin Y. Shinde^{1,2,a)}, Prasanth Prabhakaran^{1,3,b)}, Roddam Narasimha^{1,c)}

¹⁾Engineering Mechanics Unit, Jawaharlal Nehru Centre for Advanced Scientific Research, Bangalore 560064, India

²⁾Department of Mechanical Engineering, Indian Institute of Technology, Kanpur 208016, India

³⁾Department of Physics, Michigan Technological University, Houghton 49931, USA

^{a)}Electronic mail: sachin@iitk.ac.in

^{b)}Electronic mail: prasantp@mtu.edu

^{c)}Electronic mail: roddam@jncasr.ac.in

Abstract

The entrainment of ambient fluid into a turbulent shear flow has been a topic of wide interest for several decades. To estimate the entrainment of ambient fluid into turbulent jet, it is essential to define the boundary of the jet. The question arises as to what should be the appropriate criterion to determine the edge of the turbulent jet. From the present DNS simulations, we observe that there is a need to define two boundaries for the turbulent jet, namely, the Rotational/Irrotational (R/IR) interface termed here as “Outer boundary” and the Turbulent/Non-Turbulent (T/NT) interface as “Inner boundary”. The main aim of the present paper is to identify the need for defining the two boundaries for the jet. We also present some interesting observations of the jet flow, essentially on self similarity and self preservation.

1 Introduction

The entrainment of ambient fluid into a turbulent shear flow has been a topic of wide interest for several decades. The study on entrainment was inspired by a striking instantaneous shadowgraph of the turbulent wake of a bullet traveling at supersonic speeds carried out by Corrsin & Kistler (1955). To understand the several facets of the entrainment mechanism, the jet has been the most widely studied turbulent shear flow (experiments on round jets reported by Westerweel *et al.* (2002), Wolf *et al.* (2012); DNS results on a temporal round jet by Mathew & Basu (2002), on a temporally evolving plane jet by van Reeuwijk & Holzner (2014) and on a spatially developing plane jet by da Silva & Taveira (2010)).

To estimate the entrainment of ambient fluid into turbulent jet, it is essential to define the boundary of the jet. The question arises as to what should be the appropriate criterion to determine the edge of the turbulent jet. From the present DNS simulations, we observe that there is a need to define two boundaries for the turbulent jet, namely, the Rotational/Irrotational (R/IR) interface termed here as “Outer boundary” and the Turbulent/Non-Turbulent (T/NT) interface as “Inner boundary”.

The main aim of the present paper is to identify the need for defining the two boundaries for the jet. We begin with providing the details of the direct numerical simulation (DNS) and its validation. We also present some interesting observations of the jet flow, essentially on self similarity and self preservation. This is followed by a detailed discussion on the inner (T/NT) and outer (R/IR) boundaries. We conclude by presenting a summary of the findings.

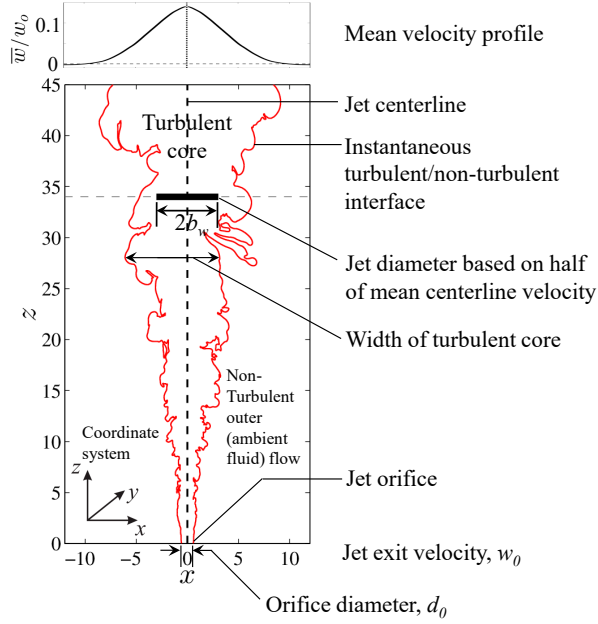


Figure 1: Schematic of an axial section of the jet flow to illustrate the main terminologies and notations, see main text for additional details.

2 DNS details

Figure 1 shows a schematic of an axial section of the jet, where d_0 represents the orifice diameter from which the jet issues with a top hat velocity profile characterized by a uniform jet exit mean velocity \bar{w}_0 . The flow is governed by the incompressible Navier-Stokes equations (in non-dimensional form with \bar{w}_0 and d_0 as velocity and length scales respectively),

$$\nabla \cdot \mathbf{u} = 0, \quad (1)$$

$$(\partial \mathbf{u} / \partial t) + (\mathbf{u} \cdot \nabla) \mathbf{u} = -\nabla p + (1/Re) \nabla^2 \mathbf{u}, \quad (2)$$

where \mathbf{u} , p represent the flow velocity vector and pressure respectively, and $Re = \bar{w}_0 d_0 / \nu$ is the Reynolds number ($= 2400$ in the present simulations), and ν is the kinematic viscosity of the fluid. Unless otherwise specified, all distances, velocities and time presented in this article are non-dimensionalized with d_0 and \bar{w}_0 as scales, and vorticity with the time-averaged local scales at height z , *viz.*, mean centerline velocity $\bar{w}_c(z)$ and mean half-velocity half-width $\bar{b}_w(z)$ at $w = \bar{w}_c/2$.

The Navier-Stokes equations are solved using an extension of Harlow & Welch's scheme (Harlow & Welch, 1965) to non-uniform grids as proposed by Verstappen & Veldman (2003), using a second-order finite volume framework. The governing equations are integrated in time using the second-order Adams-Bashforth scheme with a time step $\Delta t = 0.005$ flow unit. A non-uniform Cartesian mesh is used to resolve all the relevant scales in the turbulent part of the flow-field. The velocity and pressure variables are stored in a staggered arrangement to prevent pressure-velocity decoupling. The pressure variable is stored in the cell center and the velocity components are stored on the cell faces (Harlow & Welch, 1965). More details on the scheme and the code are discussed in Prasanth (2014). The computational domain extends up to $z = 55$ in the streamwise (z) direction and -50 to $+50$ in the cross-stream directions (x, y). The total grid size is $480 \times 480 \times 600$ in the x, y and z directions respectively (yielding 138 million grid points). In the streamwise direction, the grid size varies from 0.05 at the orifice to 0.18 at the outflow. In the cross-stream plane the grid is uniform (of size 0.05) from $x, y = -9.25$ to $+9.25$, thus ensuring

adequate resolution in the turbulent core; beyond this the grid is gradually stretched towards the lateral side walls. The simulation took up to $t = 900$ to attain a stationary state. Data for computing flow statistics was acquired over the time interval $900 < t < 2650$. The simulation was run on 108 nodes of the 360 TF supercomputer at CSIR-4PI, Bangalore, India.

The bottom plane at $z = 0$ outside the orifice is treated as a no-slip wall in the plane of the orifice exit. A fixed, uniformly distributed noise of 5% of w_o with zero mean is superposed on the top-hat velocity profile at the orifice in order to trip the flow to a turbulent state. The noise is superposed only on the streamwise velocity component, and at a random set of points chosen from a uniform distribution over the orifice area. At the outflow boundary, we use the zero normal derivative condition for all the variables, with a layer of viscous padding from $z = 52$ to $z = 55$ to ensure smooth exit of the turbulent flow from the computational domain. The lateral boundaries of the computational domain are also treated as no slip walls, but (at $x, y = \pm 50$) they are sufficiently far away from the jet axis to have any significant effect on the momentum balance. The main software used for the post-processing of the data is Matlab-2014a. Other details about the solver are discussed in Prasanth (2014).

Notice that, unless otherwise specified exclusively, all the data will be presented in non-dimensional form. The scales used for non-dimensionalization are: the orifice diameter d_o for the distance, the jet exit velocity at the orifice w_0 for velocity, and d_o/w_0 for time. Vorticity is non-dimensionalized by time averaged local scales, *viz.*, \bar{w}_c/\bar{b}_w , where \bar{w}_c is the local maximum centerline velocity and \bar{b}_w is the mean half-velocity half-width of the jet. Note that, however, for the sake of brevity, we have used the variables without an asterisk (as a superscript) or not dividing by the non-dimensional scale, in both the text as well as figures; e.g. unless exclusively mentioned ‘ q ’ represents a non-dimensional form of a quantity ‘ q ’.

2.1 Validation

Figure 2 shows the flow structure of the jet at one instant. It is evident that the jet surface, and thus the jet boundary, are highly convoluted.

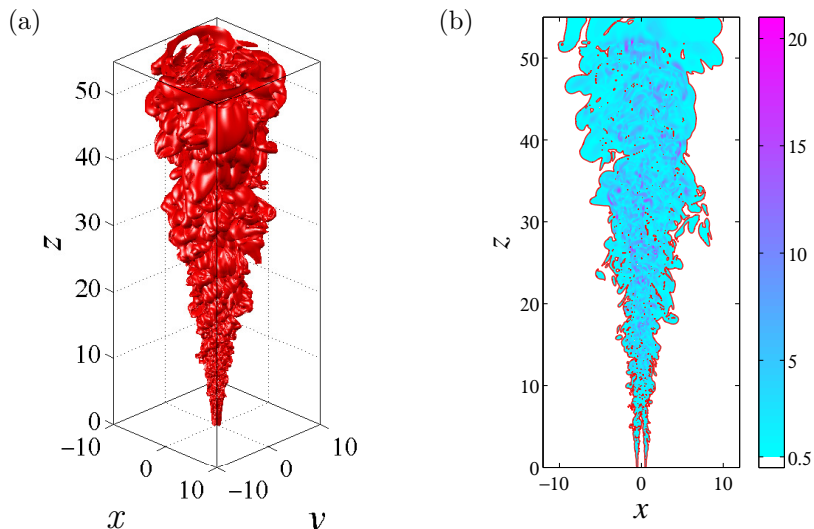


Figure 2: Instantaneous snapshot of vorticity field of a round incompressible turbulent jet at time $t = 1995$ flow units since the inception of the flow, obtained from the direct numerical simulation. (a) Iso-surface of vorticity magnitude at a threshold of 0.5. (b) An axial section of the flow.

Figures 3(a) and 3(b) show the streamwise variation of the inverse of the mean centerline velocity and the mean-half-velocity half-width respectively. We see that the inverse of the centerline velocity increases linearly with the streamwise distance. The slope from the data shown in Fig. 3(a) is 0.17, which is

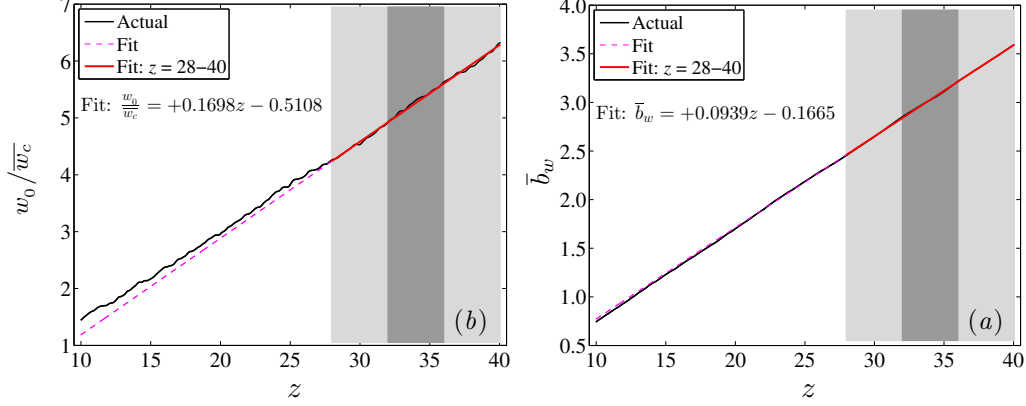


Figure 3: Variation with the streamwise distance of the time-azimuthal averaged flow data: (a) inverse centerline velocity; (b) jet half-velocity width. The light and dark grey rectangle indicate respectively the self-similar and self-preservation region (to be discussed in section 2.2).

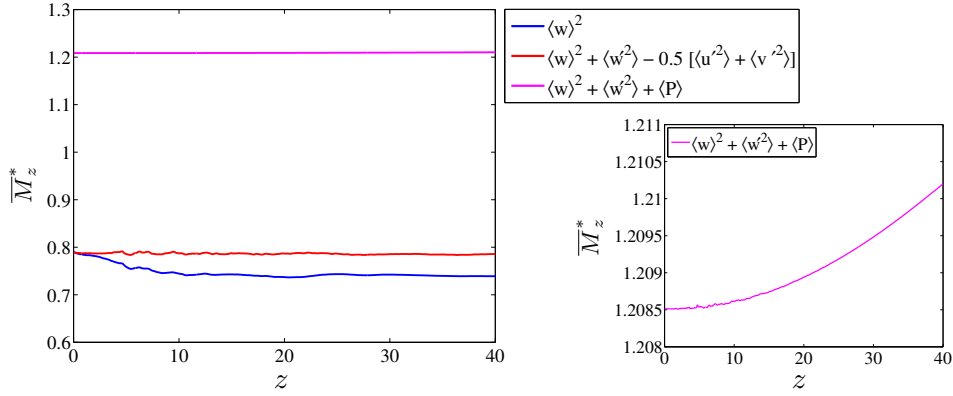


Figure 4: Variation with the streamwise distance of the mean streamwise momentum flux in the jet normalized by the inlet conditions, defined in different ways. On the right, the plot shows the zoomed-in view of the momentum flux including the pressure term calculated directly from the DNS data. The variation in normalized momentum flux over a downstream distance of 40 orifice diameters is about 0.0017.

comparable to the experimental values of 0.16 (Panchapakesan & Lumley, 1993) and 0.17 (Hussein *et al.*, 1994). Figure 3(b) shows that the half-velocity half-width of the jet increases linearly with streamwise distance and the rate of increase is 0.094, which is comparable to the experimentally measured value of 0.097 by Westerweel *et al.* (2009).

Figure 4 shows the variation of streamwise momentum flux with the streamwise distance. The net momentum flux $\int (\overline{w^2} + \overline{w'^2} - 0.5[\overline{u'^2} + \overline{v'^2}])dS$, where the overbar denotes time average, prime denotes fluctuation (Hussein *et al.*, 1994), and the domain of integration is $-50 \leq x, y \leq 50$, is conserved to better than 99% over the whole domain in the z direction.

2.2 Self-preserving flow

We observed that the jet attains a state of self-similarity at a distance of $z/d_0 \approx 28$. The flow remains self-similar up to $z/d_0 \approx 40$. In this region, the streamwise velocity profiles show a remarkable collapse when normalized with local centerline velocity and \bar{b}_w as shown in Fig. 5(a). It is found that the jet is in a self-similar state over the range $28 \leq z \leq 40$ to within 0.6% in the mean velocity (\bar{w}/\bar{w}_c). However, for the flow to be “self-preserving”, both streamwise velocity profiles as well as the Reynolds shear stress should show a close collapse, when normalized with the same local scales, i.e., the centerline velocity and

\bar{b}_w . We found that the jet is in an equilibrium or self-preserving state, *i.e.*, mean velocity and Reynolds stress are self-similar over the range $32 \leq z \leq 36$, the maximum in $(\overline{w'^2}/\bar{w}_c^2)^{0.5}$ (not shown here) and Reynolds shear stress $-\overline{w'w'_r}/\bar{w}_c^2$ (Fig. 5(b)) vary less than 1% and 1.5% respectively. Therefore, we will confine our analysis to the self-preserving region. We observed that there are negative velocities outside the core of the jet due to recirculation; however they are negligibly small, the maximum being -0.0053 of the centerline velocity as shown in the bottom inset of Figure 5(a).

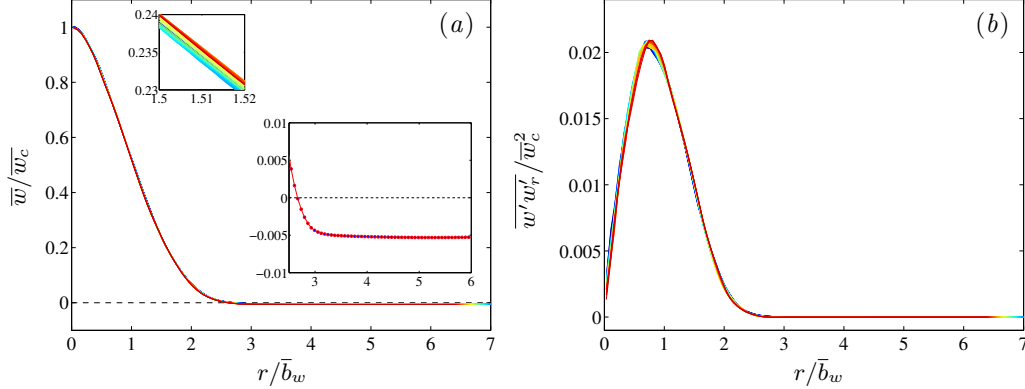


Figure 5: Variation in the radial direction of the time and azimuthally averaged flow data. The data are plotted for all the 33 stations spanning the self-preservation region, namely, from $z = 32$ to 36 . (a) Axial velocity profile. Top inset shows a zoomed-in view of a particular portion of the velocity profiles to emphasize that there are 33 lines which fall on top of each other. Bottom inset shows the zoomed-in view between 2.5 to 6 on the abscissa, showcasing primarily the negative axial velocities outside the core of the jet; notice that the data here is averaged over all 33 stations. (b) Reynolds shear stress profiles.

3 Defining the jet boundary: Two boundaries?

The boundary of the turbulent jet is defined by putting threshold on the vorticity modulus $|\omega|$. Figure 6 shows the contours of vorticity magnitude within the core of the jet in axial (Figure 6(a)) and diametral (Figure 6(b)) planes. In both the axial and diametral planes, the jet boundaries are plotted at five different thresholds on $|\omega|$, ranging from 0.1 to 0.5.

In order to locate the boundary of a turbulent jet, we look at the variation of the vorticity modulus ($|\omega|$) across the jet diameter; for example, Figure 7 shows that the instantaneous variation of vorticity magnitude plotted along the radial direction at various radial locations. It is evident from the figure that the irrotational and rotational fluid regions are separated by a very thin and sharp interface. Vorticity shows wild fluctuations within the core of the jet.

The definition of the edge is determined as a characteristic value of $|\omega|$ connected with the interface layer of relatively rapid change that is encountered as a test point moves inward toward the jet core from the ambient (nearly) irrotational flow.

Figure 8(a) displays the variation of the total vorticity modulus $|\omega|$ across the jet diameter at $z = 34.05$. For comparison the magnitude of the mean flow vorticity is also shown. It is first of all seen that the fluctuating vorticity $|\omega|$ in the core can be an order of magnitude larger than the time mean flow vorticity.

If we take a test point that moves towards the turbulent core from the ambient in the right in 7(a), we see that $|\omega|$ remains nearly constant till the test point crosses $x \approx 7$ where it encounters a sudden and relatively rapid change in $|\omega|$ from nearly 0.1 to 4, thereafter showing wild fluctuations till it reaches $x \approx -4.5$ where $|\omega|$ drops steeply all the way to about 0.5, then becomes less steep, and finally takes

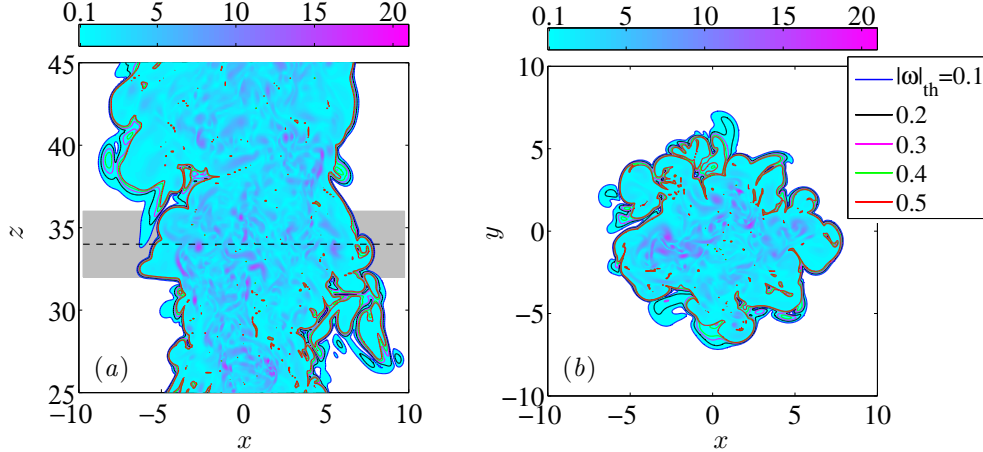


Figure 6: Instantaneous vorticity snapshot at $t = 1995$ flow units since the start of the flow, for vorticity magnitude threshold of 0.1. (a) shows an axial section at $\Phi = 0^\circ$ and (b) shows a diametral section at $z = 34$. Also shown are the jet boundaries at various vorticity magnitude thresholds from 0.1 to 0.5 in steps of 0.1. In (a), the gray rectangle highlights the self-preservation region, and the dotted black line at $z = 34$ shows the location which lies in the middle of the self-preservation region, and where the vorticity contours in (b) are drawn.

the form of two noticeable but smooth bumps, the one farther away being the bigger, beyond which $|\omega|$ remains nearly constant at a small value. We will shortly demonstrate (from comparison with Figure 8 (b)) that these two bumps correlate with the outer buffer zone with its small but apparently non-turbulent vorticity. For several vorticity profiles studied, it is observed that the $|\omega|$ invariably shows a rapid and sudden increase beyond $|\omega| = 0.5$; however, up to $|\omega| = 0.5$ the vorticity profile shows both rapid increase (e.g. at $x \approx 6.5$) as well as slow increase (e.g. $x \approx -5$). In order to explore the physical picture of the flow near the jet boundary, we plot the vorticity $|\omega|$ field in axial sections near the left and right boundaries of the jet as shown in Figure 8(b). We also draw three boundaries defined by a threshold on $|\omega| = 0.1, 0.5, 1.0$ respectively. We observe that the two boundaries for $|\omega| = 0.5, 1$ mostly lie close to each other except in a small region $2 < x < 7$ and $30.5 < z < 31$. However, the separation between boundaries defined by $|\omega| = 0.5$ and $|\omega| = 0.1$ show a different trend: the separation between these two boundaries can be very small at some places, but can vary appreciably at certain other locations along the boundary of the jet; for example, in Fig. 8(b) the two boundaries are close to each other in some areas (e.g., $-8 < x < -6$ and $38 < z < 45$) and well separated in others (e.g., $-8 < x < -3$ and $31 < z < 38$). Figure 9 shows the vorticity field and the jet boundaries defined based on two thresholds (namely 0.1 and 0.5) in a diametral plane. Just as in the case of the axial plane, it is clearly visible in Figure 9 that the two boundaries are quite close to each other at some places and widely separated at others.

In the region bounded by $|\omega| = 0.5$ and $|\omega| = 0.1$, vorticity shows interesting behaviour - while at some places it increases rapidly, it shows very slow spatial frequency of variations some other places. This lays the basis to define two boundaries for the jet instead of a single boundary.

Based on extensive studies of these vorticity profiles across the edge, it is found convenient to introduce two distinct edges or boundaries of the jet. The first is located at $|\omega| = 0.5$, beyond which $|\omega|$ varies rapidly to 1.0 or above in the turbulent core. This defines the turbulent / non-turbulent (T/NT) ‘inner’ boundary of the turbulent jet. For reasons that will be clear shortly, we find it necessary to define an ‘outer’ boundary at $|\omega| = 0.1$, which similarly locates the rotational / irrotational (R/IR) boundary of the jet. The contour surfaces $|\omega| = 0.1$ and 0.5 will thus be referred to in the sequel as the ‘outer’ (R/IR) and ‘inner’ (T/NT) boundaries of the jet respectively. As expected, the edges of the jet are highly convoluted (especially the inner boundary, which is a fractal curve (Sreenivasan & Meneveau, 1986; Sreenivasan

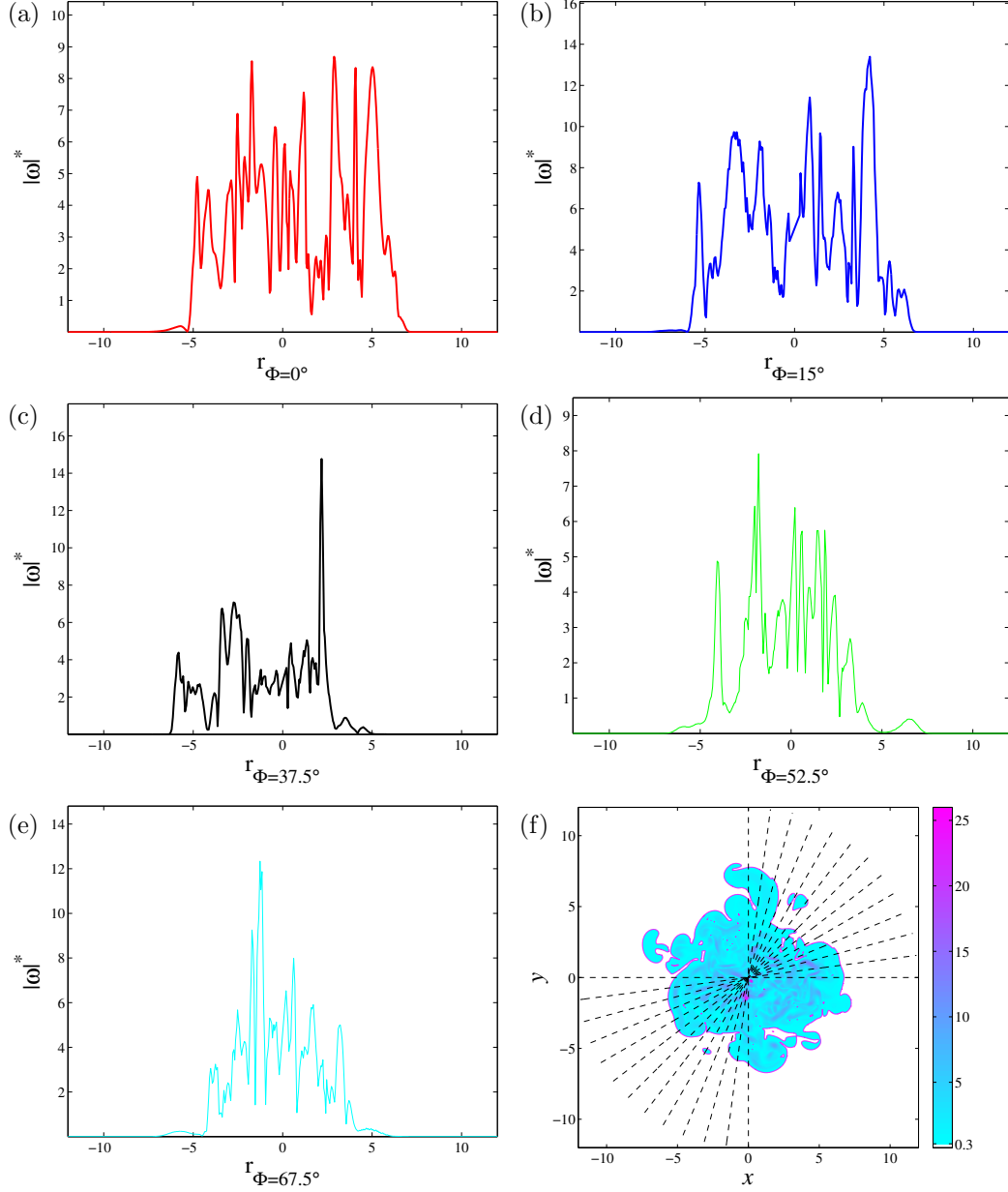


Figure 7: (a - e): Instantaneous vorticity magnitude profiles in axial sections at $z = 35$ and $t = 1995$: (a) $\Phi = 0^\circ$; (b) $\Phi = 15^\circ$; (c) $\Phi = 37.5^\circ$; (d) $\Phi = 52.5^\circ$; (e) $\Phi = 67.5^\circ$. Vorticity is non-dimensionalized using the local scales, i.e. \bar{w}_c/\bar{b}_w . (f) shows the vorticity contours in a diametral plane at $z = 35$; the jet edge is plotted at a threshold of $|\omega|_{\text{th}=0.3}^*$. The broken radial lines are drawn in an interval of 7.5° between $\Phi = 0^\circ - 90^\circ$. The vorticity profiles in (a) to (e) are plotted along the dotted lines at respective radial locations.

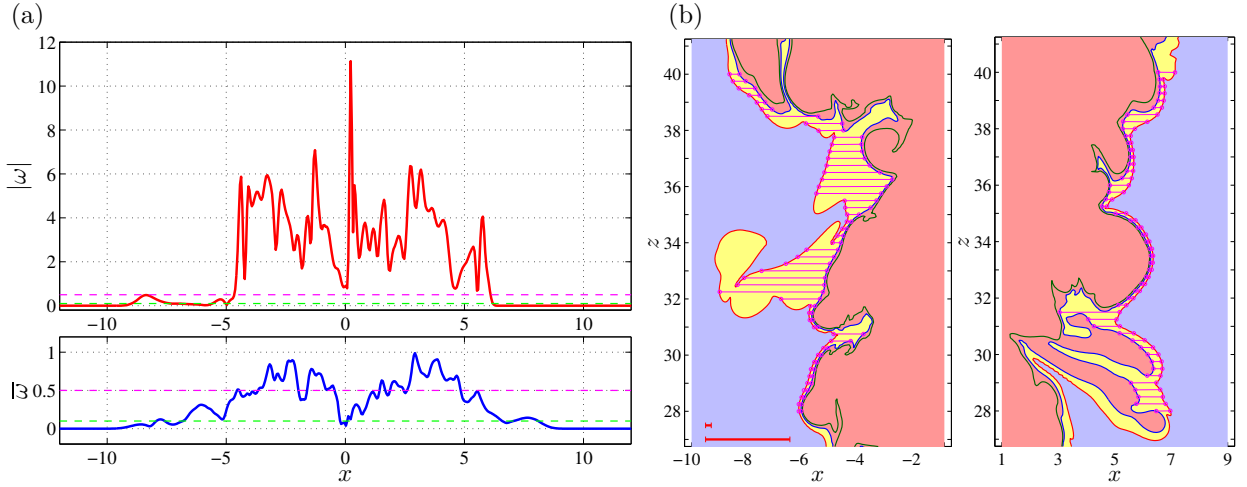


Figure 8: (a) Typical variation of the normalized instantaneous vorticity modulus $|\omega|$ (in red) at $t = 925$, compared with the time-averaged vorticity modulus, $|\bar{\omega}|$ (in blue). The broken horizontal lines are marked at 0.1 (green) and 0.5 (pink). The bumps within $-10 < x < -5$ correspond to the two intersections of the line $z = 34.05$ with the outer viscous buffer zone (yellow region in the left panel of b). (b) Axial section in the xz plane at $t = 925$. The $|\omega| = 0.1$ and 0.5 contours in the axial cross section of the jet showing the wide variability in the separation distance between the two contours that bound the yellow region (viscous buffer zone); lighter reddish region is the turbulent core, lighter lavender region is the ambient. The red, blue and dark green boundaries are marked respectively at thresholds $|\omega| = 0.1, 0.5, 1$. The thick red horizontal lines at the bottom in the left panel show 5η (short line) and 5λ (long line).

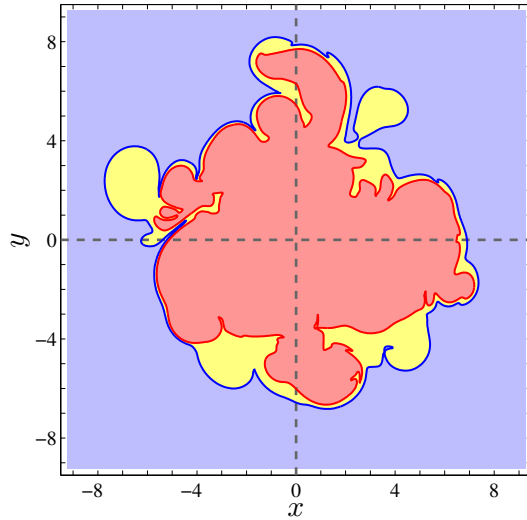


Figure 9: Instantaneous sectional view of the jet in a diametral plane at $z = 35$ showing the boundary of the jet at $t = 1995$ for two thresholds, namely, 0.1 (blue) and 0.5 (red). These boundaries demarcate the flow into three regions: Irrotational (violet), Viscous (yellow) and Turbulent (light red).

et al., 1989)). When the separation between the inner and outer boundaries is large, we call the region between them an ‘outer buffer zone’.

It would be worthwhile to study the variation of separation distance between inner and outer boundaries. Figure 8(b) shows how the distance between the two boundaries varies along the inner boundary of the jet. One simple measure of this distance is the separation along the x axis from the inner to the outer boundary on either side of the jet. It is seen that this inter-boundary separation varies from 0.090 to 3.67 in the left boundary and from 0.077 to 2.13 in the right boundary. For comparison, estimates of the two relevant scales in the problem, namely, the Kolmogorov length (η) and the Taylor microscale (λ) at $z \approx 33$, $x, y = 0$ are shown in Fig. 8(b). It is seen that inter-boundary separation varies from the order of the Kolmogorov scale to the Taylor microscale; however, the changes in $|\omega|$ from 0.5 toward 1.0 and above in the turbulent core is almost always sharp, and has a length scale comparable to the Kolmogorov scale. In the light of the many discussions on this issue in the literature (da Silva & Taveira, 2010; da Silva & dos Reis, 2011; da Silva & Pereira, 2008; Westerweel *et al.*, 2009; Hunt *et al.*, 2006), we conclude that both scales seem to have a role to play, from the sharp T/NT interface layer of thickness $\mathcal{O}(\eta)$ to the larger lateral extent of the viscous buffer zone with a dimension of order λ . Understanding the role of these different scales, and the question of whether this difference in scales persists at higher Reynolds numbers requires further investigation.

Note that there have been other proposals as well for defining two boundaries, but, using slightly different criteria; for example, van Reeuwijk & Holzner (2014) used thresholds on enstrophy to define inner and outer boundaries for a temporal plane jet. Their inner boundary, that separates the turbulent core from the buffer region, represents the enstrophy threshold for which the interface propagation velocity v_n is zero, and the outer boundary, that separates the viscous superlayer (VSL) from the buffer region, represents the threshold below which the enstrophy production is negligible. (Also, they define a buffer zone which possibly is inward of our inner boundary, and will here be called the ‘inner buffer zone’.) Note that the thresholds used by van Reeuwijk & Holzner (2014) in the case of a temporal plane jet at $Re = 5000$ for defining the boundaries are not applicable in our case as the thresholds are a function of Reynolds number and also of the dimensionality and nature of the flow.

3.1 Nature of vorticity field between T/NT and R/IR interfaces

Figure 10 shows the time evolution (over $930 \leq t \leq 965$) of a part of the jet ($32 < z < 36$) that is accurately self-preserving. Region A hardly changes in shape or in vorticity range over this whole time interval. On the other hand, region B keeps continuously shrinking, and has disappeared at $t = 965$. This disappearance is largely due to the outward motion of the inner boundary till, in (d), the two boundaries are very close to each other in the interface above $z = 34$. Region C undergoes minor changes in shape, in part again because of the outward movement of the inner boundary. Between (a) and (d) it is seen that the turbulent core has expanded, with a general reduction in the larger vorticity-sparse areas seen near the boundaries in the earlier images.

Figure 11 compares the variation of $|\omega|$ with time at two points. The vorticity at the center line shows substantial variation in time, whereas that in area A in the outer buffer zone is more than an order of magnitude lower and exhibits a slow and gentle decay with hardly any fluctuation that can be associated with turbulence. This justifies why such a buffer zone can be characterized as ‘viscous’, and the structure at zone A in Fig. 10 may be called a ‘viscous tongue’, most probably a relic or fossil from an earlier excursion of in- or out-of-plane vorticity from the core or buffer zone into an ambient nearly at rest.

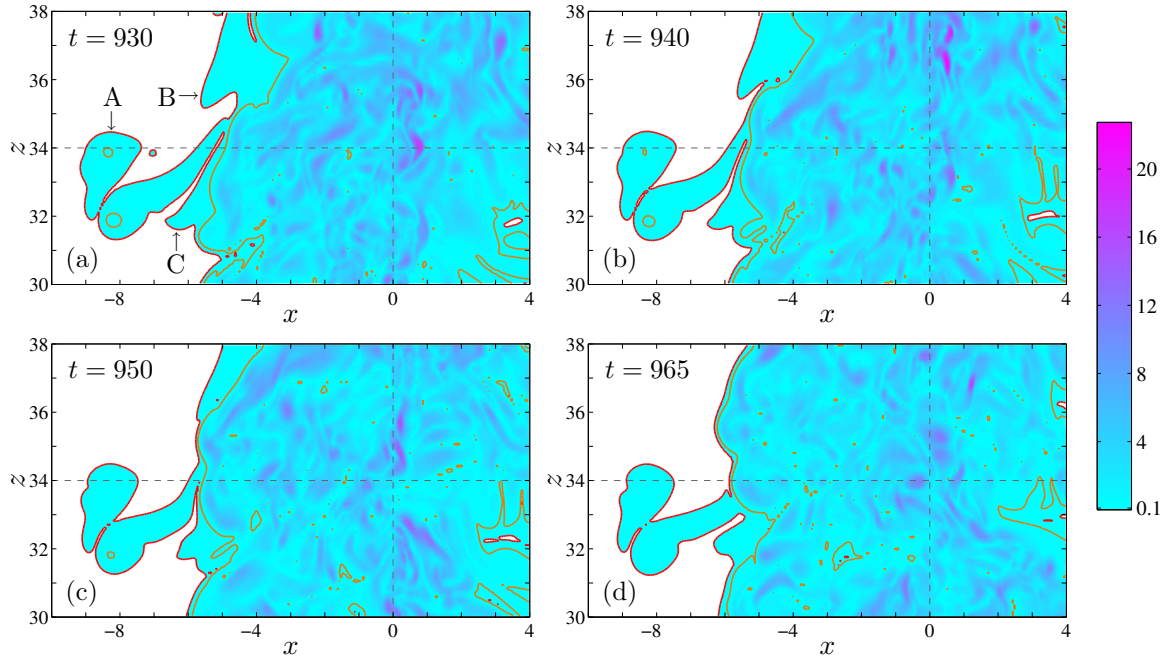


Figure 10: Temporal evolution of a part of the jet. Three areas in the figure labeled as A, B and C illustrate important features of the evolution (see text for discussion).

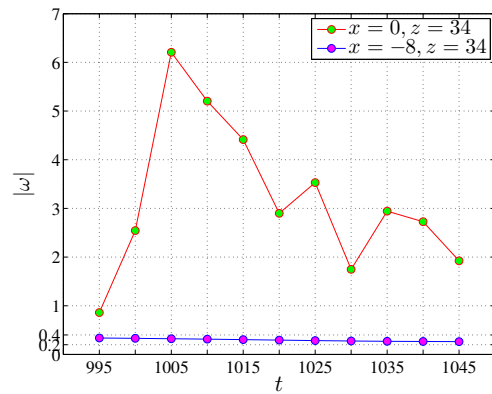


Figure 11: Temporal variation of the total vorticity modulus at two points in the plane $z = 34$, one on the centerline $(0, 0, 34)$ and the other at $(-8, 0, 34)$ in the outer buffer region between the inner and outer boundaries.

3.2 Interface thickness

We are interested in finding out the thickness of the jet interface, i.e., the interface which separates the rotational mass, which constitutes the turbulent jet fluid, and the irrotational mass which is outside the jet core.

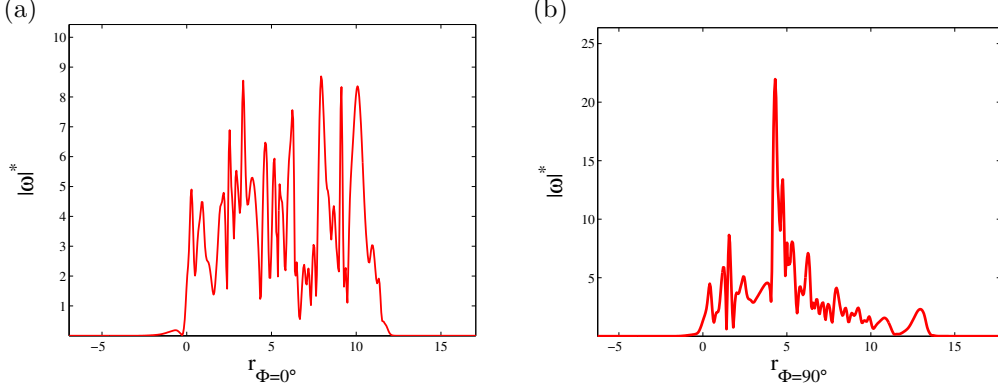


Figure 12: Instantaneous vorticity magnitude profiles at $z = 35$ in two axial sections: (a) $\Phi = 0^\circ$; (b) $\Phi = 90^\circ$; $t = 1995$. Vorticity is non-dimensionalized using the local scales, i.e. \bar{w}_c/\bar{b}_w . Note that for doing the edge-based averaging, the origin of the coordinates system in the radial direction is shifted to the edge of the jet on the left side.

For this purpose, we do edge-based time averaging of the vorticity, which essentially means shifting the origin of the coordinate system in radial direction to the jet interface where the vorticity profile shows a very sharp and steep decline, and then perform the averaging; for example, see Figure 12 wherein the origin of the coordinate system in radial direction is shifted to the left interface of the jet. Figure 13 shows the vorticity profiles for the edge-based time averaged data wherein the edge is fixed at a vorticity magnitude threshold of 0.5. similar kind of vorticity profiles are presented in Westerweel *et al.* (2009). Figure 13(a) shows that the vorticity profiles show a close collapse at the interface when scaled with the half-velocity width. Figure 13(b) shows a zoomed-in view of figure 13(a), focused near the interface. If we normalize the vorticity profiles in a way similar to that in the case of mixing layers, then we observe an even tighter collapse in the interface region, as seen in Figure 13(c). Based on the characteristics of the vorticity profiles near the interface, but towards the core of the jet, we identified three regimes, namely overshooting, rising and flat profiles, as shown in Figure 14.

The interface width in our case is about 0.1 of the half-velocity width (see Figure 13). It is important to see how much is the interface thickness when compared with the Taylor and Kolmogorov scales. The important question to ask is: among the two scales, with what does the interface thickness scale? The Kolmogorov and Taylor scales are shown in Figure 15. Our simulations showed that the interface thickness is about double the Kolmogorov scale whereas it is about one fifth of the Taylor microscale.

4 Interface tracking and entrainment

Figure 2(a) shows a three-dimensional view of the round turbulent jet at one time instant. Figure 16 shows the 3-D view of the jet in the self-preserving region, especially showing the internal structure of the jet. The threshold used for identifying the jet boundary is $|\omega| = 0.5$. Both the figures show that the jet boundary is quite jagged and convoluted. Figure 16 shows that there are some isolated patches of vorticity within the core of the jet as well as in the ambient. In order to identify these vorticity patches, we define the following terms.

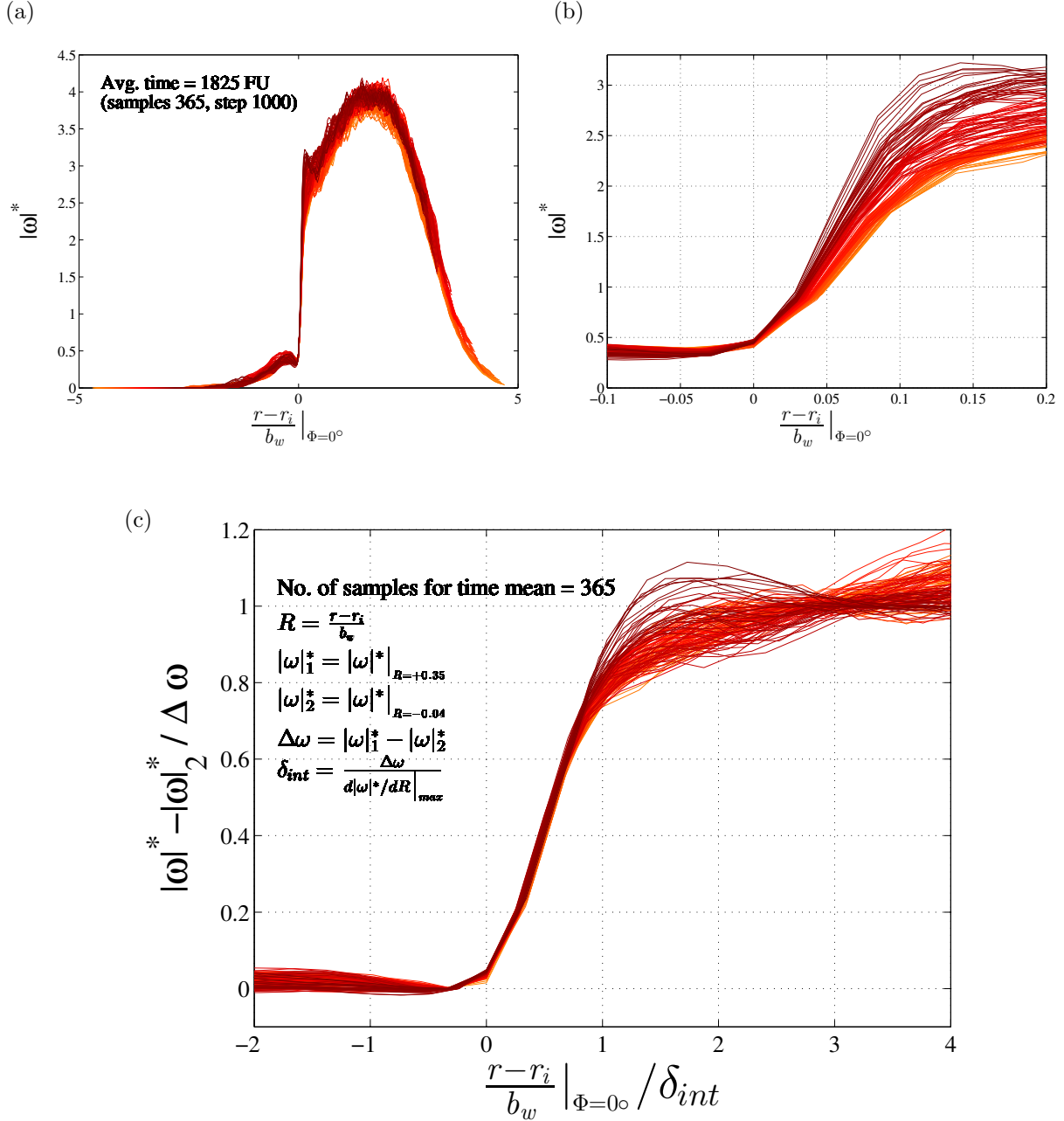


Figure 13: Edge-based time mean data (see text for details); $z = 25 - 40, \Phi = 0^\circ$. The data is averaged over 1825 flow units. The edge is defined at $|\omega|_{th} = 0.5$. Vorticity is normalized with the local scales, namely, \bar{w}_c and \bar{b}_w . Radial profiles of vorticity magnitude profiles: (a) across the entire section of the jet; (b) zoomed in near the interface; (c) zoomed in view with different normalization as mentioned in the legend.

- **Jet boundary/edge:** This is an iso-surface (in three dimensions) or a iso-contour (in two dimensions) which is defined based on a threshold set on the vorticity magnitude that marks the boundary on the turbulent jet.
- **Well/Gulf/Incursion:** A narrow region of the non-turbulent outside fluid making deep penetration into the turbulent jet.
- **Lake:** Isolated region of non-turbulent fluid present within the core of the turbulent jet.
- **Island:** Isolated region of turbulent fluid present within the expanse of outside non-turbulent fluid.

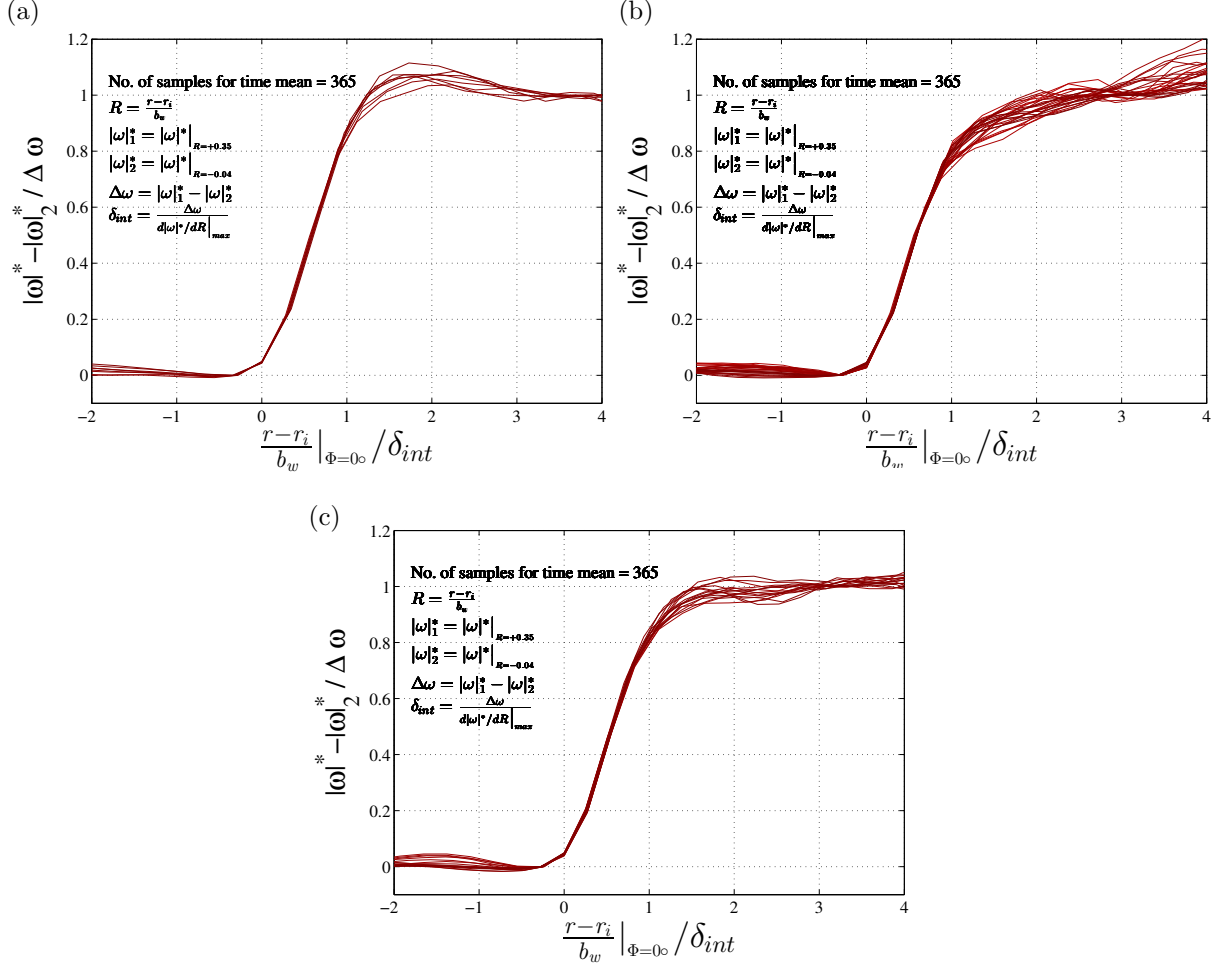


Figure 14: Three regimes of the vorticity magnitude profiles shown in figure 13(c): (a) overshoot: $z = 39 - 40$; (b) rising: $z = 29 - 32$; (c) flat: $z = 37 - 39$.

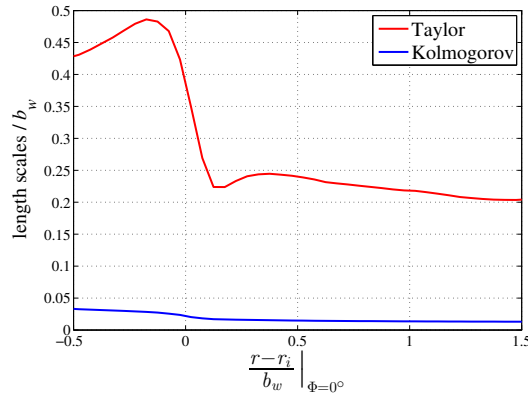


Figure 15: Variation of Kolmogorov and Taylor length scales at $z \approx 33$.

Figure 16 shows an isometric view of a section of the jet at two different instants. It is clearly evident from the figures that there are isolated ‘lakes’ of non-turbulent fluid marked with blue color in the figures. Also, the presence of isolated ‘islands’ of turbulent fluid can be seen outside the boundary of the jet. Note that, these islands can be a part of the turbulent jet which looks isolated in the section chosen here (and hence qualified as islands), but might be connected to the jet somewhere else along the axial direction; for

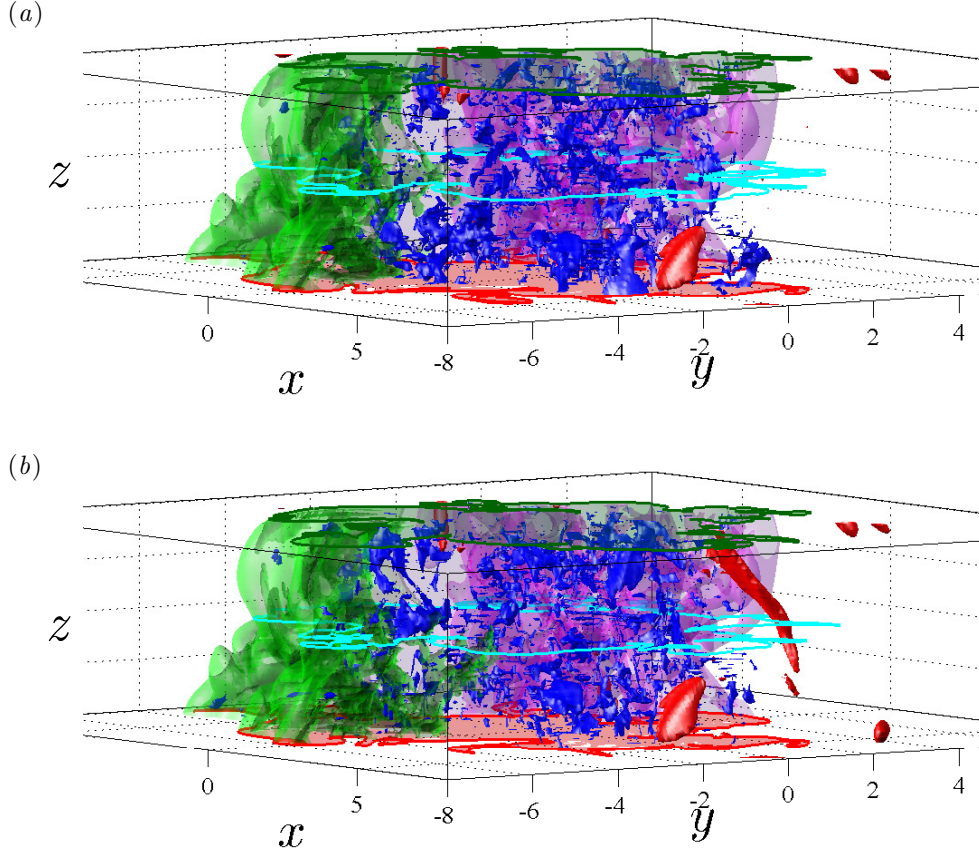


Figure 16: Instantaneous 3D sectional view of Jet depicting Islands (red) and Lakes (blue). The jet envelope defined by a vorticity fluctuations magnitude threshold at 1.0 is shown by pink and green surface in the first and second quadrants. (a) $t = 399000$; (b) $t = 399550$.

example, the two red patches seen near the upper surface on the right side in Figures 16(a,b). However, these figures also reveal that there are totally disconnected and isolated blobs of turbulent fluid lying outside the jet boundary; for example, the one red blob near the bottom surface in Figure 16(a), two red blobs near bottom surface and one long red tongue, starting near the upper surface and running all the way towards the bottom surface in Figure 16(b) are the example of islands. The lakes and islands will appear as the disconnected areas in a two-dimensional cross-section; see for example Figure 17. To get the true turbulent mass flux in a jet, the calculation should exclude the contributions from the irrotational mass in islands and lakes as they do not constitute turbulent flow.

Tracking the jet boundary in three dimensions is indeed challenging. Therefore, we began with a two-dimensional (2D) case having fairly simple geometry, and then extended the methodology to the complex situations in 2D. Once we ensured that the methodology works fine for the two-dimensional case, we have extended it in three-dimensions (3D). However, note that it is not a straight forward extension from 2D to 3D.

The first step towards the boundary-tracking is to get rid of the small debris of islands and lakes, which actually do not form a part of the jet boundary. For instance, Figures 17(a1 and b1) show the jet boundary along with the Islands and Lakes in a 2D axial plane for two different vorticity thresholds. Figures 17(a2 and b2) show a cleaned-up jet boundary for a 2D case. In 3D, removing Islands and Lakes is quite challenging. However, it is possible to generate the jet surface free from Islands and Lakes.

In order to understand the entrainment mechanism of the ambient irrotational fluid into the turbulent core, we are analyzing the flow field both within and outside the turbulent core. Figure 18 velocity and

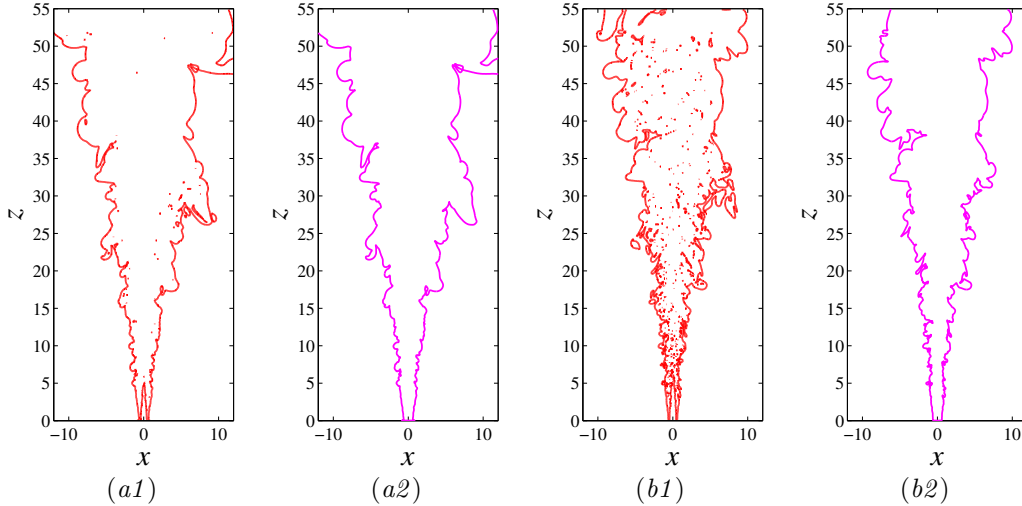


Figure 17: Instantaneous sectional view of the jet in an axial plane at $\phi = 0^\circ$ showing the boundary of the jet at $t = 1995$ for two thresholds, namely $|\omega|_{th=0.1}^*$ (*a1*, *a2*) and $|\omega|_{th=0.5}^*$ (*b1*, *b2*). (*a1* and *b1*) show jet section showing the vorticity patches within (lake) and outside (island) of the jet core along with the jet boundary. (*a2* and *b2*) show the corresponding jet section marking only the jet edge after removal of the islands and lakes. Comparison of (*a1*) and (*b1*) clearly shows the noticeable increase in the number of islands and lakes at a higher threshold.

vorticity fields at one instant in an axial plane. It appears that the fluid is entrained in to the jet largely through the deep incursions, which we term as “Wells”. Figure 19 shows the velocity and vorticity fields in a diametral plane, for the same time instant. Further analysis to gain understanding on entrainment process is in progress.

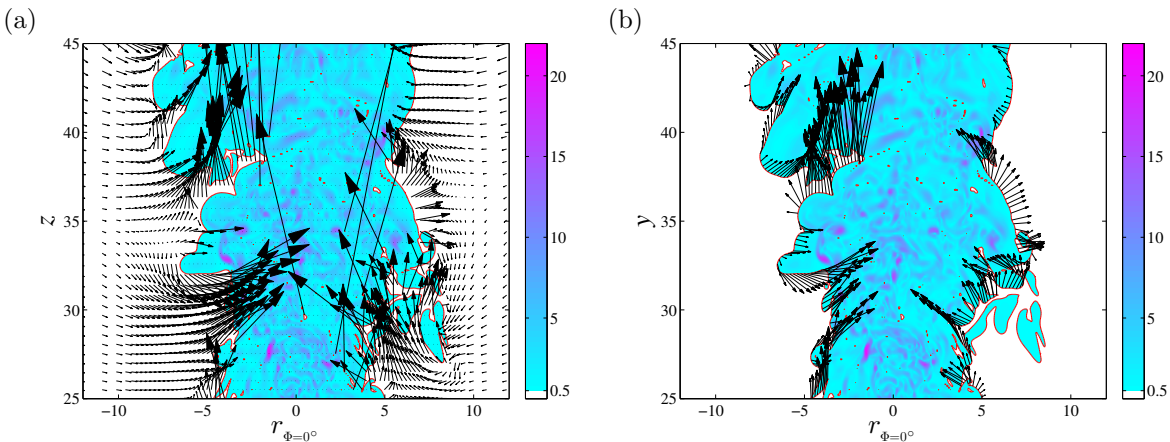


Figure 18: Instantaneous velocity and vorticity fields in an axial plane ($\Phi = 0^\circ$) at $t = 2000$. The jet boundary is at $|\omega|_{th} = 0.5$. (a) Note that the velocity vectors are plotted only outside the jet boundary. (b) shows the flow velocity only at the jet boundary.

5 Summary

Direct Numerical Simulation (DNS) has been carried out on an incompressible turbulent round jet at a Reynolds number of 2400 (based on orifice diameter d_0 and mean exit velocity \bar{w}_0 at floor level $z = 0$ inlet conditions). The validation showed that the simulations are of high quality in terms of self-similarity and conservation of momentum. We identified an accurately self-preserving region in the jet that spans over 4 orifice diameters ($32 \leq z \leq 36$). We also demonstrated that we need to define two boundaries for the

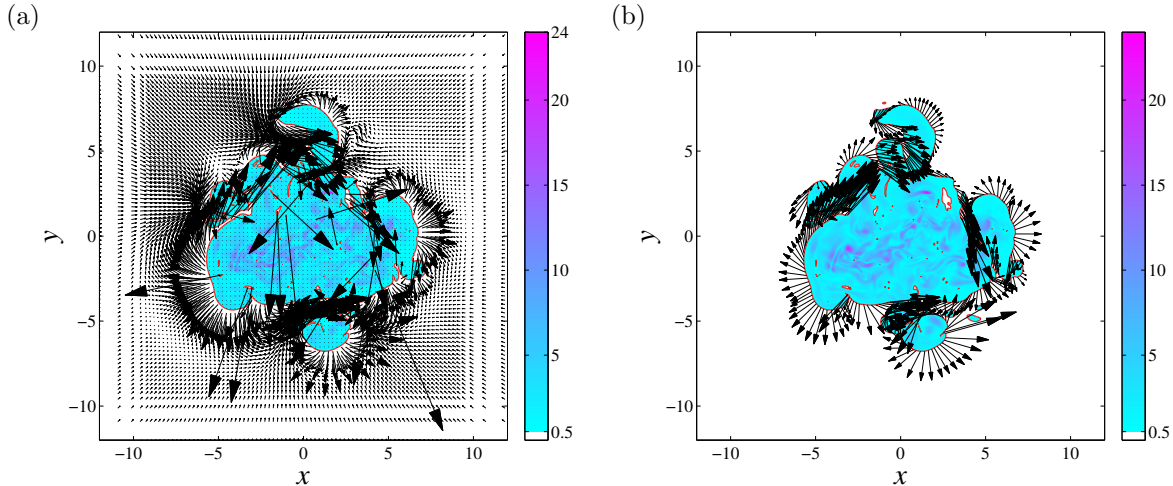


Figure 19: Instantaneous velocity and vorticity fields in a diametral plane at $z = 35$ at $t = 2000$. The jet boundary is at $|\omega|_{th} = 0.5$. (a) Note that the velocity vectors are plotted only outside the jet boundary. (b) shows the flow velocity only at the jet boundary.

jet: the “inner” boundary known as T/NT interface that isolated turbulent fluid from non-turbulent but rotational fluid; and, the “outer” boundary known as R/IR interface that demarcates between rotational and irrotational fluid. We showed that the appropriate thresholds for defining these two boundaries based on vorticity modulus are 0.1 for the outer boundary and 0.5 for the inner boundary. We showed that the fluid confined between these two boundaries is rotational but non-turbulent as it does not show any vorticity fluctuations for very long duration. We show that this fluid is often a long-lasting relic of a turbulent ‘tongue’ or island separated from the turbulent core at some much earlier time at the previous instants. We also provided the methods for identifying the boundary in 3D. The analysis on entrainment mechanism is in progress.

References

- CORRSIN, STANLEY & KISTLER, ALAN L 1955 Free-stream boundaries of turbulent flows. *Tech. Rep.*. NACA Report 1244.
- HARLOW, FRANCIS H & WELCH, J EDDIE 1965 Numerical calculation of time-dependent viscous incompressible flow of fluid with free surface. *Physics of Fluids* **8** (12), 2182.
- HUNT, JCR, EAMES, I & WESTERWEEL, J 2006 Mechanics of inhomogeneous turbulence and interfacial layers. *Journal of Fluid Mechanics* **554**, 499–519.
- HUSSEIN, HUSSEIN J, CAPP, STEVEN P & GEORGE, WILLIAM K 1994 Velocity measurements in a high-reynolds-number, momentum-conserving, axisymmetric, turbulent jet. *Journal of Fluid Mechanics* **258**, 31–75.
- MATHEW, JOSEPH & BASU, AMIT J 2002 Some characteristics of entrainment at a cylindrical turbulence boundary. *Physics of Fluids (1994-present)* **14** (7), 2065–2072.
- PANCHAPAKESAN, NR & LUMLEY, JL 1993 Turbulence measurements in axisymmetric jets of air and helium. part 1. air jet. *Journal of Fluid Mechanics* **246**, 197–223.
- PRASANTH, PRABHAKARAN 2014 Direct numerical simulation of transient cumulus cloud flow. Master’s thesis, Jawaharlal Nehru Centre for Advanced Scientific Research, India.

- VAN REEUWIJK, MAARTEN & HOLZNER, MARKUS 2014 The turbulence boundary of a temporal jet. *Journal of Fluid Mechanics* **739**, 254–275.
- DA SILVA, CARLOS B & PEREIRA, JOSÉ CF 2008 Invariants of the velocity-gradient, rate-of-strain, and rate-of-rotation tensors across the turbulent/nonturbulent interface in jets. *Physics of Fluids* **20** (5), 055101.
- DA SILVA, CARLOS BETTENCOURT & DOS REIS, RICARDO JOSÉ NUNES 2011 The role of coherent vortices near the turbulent/non-turbulent interface in a planar jet. *Philosophical Transactions of the Royal Society of London A: Mathematical, Physical and Engineering Sciences* **369** (1937), 738–753.
- DA SILVA, CARLOS B & TAVEIRA, RODRIGO R 2010 The thickness of the turbulent/nonturbulent interface is equal to the radius of the large vorticity structures near the edge of the shear layer. *Physics of Fluids* **22** (12), 121702.
- SREENIVASAN, KR, RAMSHANKAR, R & MENEVEAU, CH 1989 Mixing, entrainment and fractal dimensions of surfaces in turbulent flows. *Proc. R. Soc. Lond. A* **421** (1860), 79–108.
- SREENIVASAN, K R & MENEVEAU, C 1986 The fractal facets of turbulence. *Journal of Fluid Mechanics* **173**, 357–386.
- VERSTAPPEN, RWCP & VELDMAN, AEP 2003 Symmetry-preserving discretization of turbulent flow. *Journal of Computational Physics* **187** (1), 343–368.
- WESTERWEEL, J, FUKUSHIMA, C, PEDERSEN, JAKOB MARTIN & HUNT, JCR 2009 Momentum and scalar transport at the turbulent/non-turbulent interface of a jet. *Journal of Fluid Mechanics* **631**, 199–230.
- WESTERWEEL, J, HOFMANN, T, FUKUSHIMA, C & HUNT, J 2002 The turbulent/non-turbulent interface at the outer boundary of a self-similar turbulent jet. *Experiments in Fluids* **33** (6), 873–878.
- WOLF, M, LÜTHI, B, HOLZNER, M, KRUG, D, KINZELBACH, W & TSINOBER, A 2012 Investigations on the local entrainment velocity in a turbulent jet. *Physics of Fluids* **24** (10), 105110.